Simulation of solid-state lasers with temperature and wavelength dependent absorption and emission

Souryadeep Saha[a,c], Jacob I. Mackenzie[b], and Christoph Pflaum[a]

[a]FAU Erlangen-Nürnberg, Germany
[b]Optoelectronics Research Center, University of Southampton
[c]Erlangen Graduate School in Advanced Optical Technologies (SAOT)

ABSTRACT

Simulation of diode-pumped solid-state lasers (DPSSL) and amplifiers often do not account for the temperature and spectral dependencies of the absorption and emission cross sections of the gain medium. Typically, to track the pump absorption within the crystal, an average absorption coefficient is applied via a raytracing technique. The outcome, therefore, is an approximation of the pump absorption profile that is independent of the temperature profile within the gain medium. Here an iterative algorithm involving raytracing and Finite Element Analysis (FEA) is demonstrated in the simulation of neodymium(Nd) and ytterbium(Yb) doped yttrium aluminium garnet(YAG) single crystal fiber (SCF) gain media. The algorithm calculates the local temperature, associated absorption coefficient and hence temperature-dependent pump absorption. This allows for a more accurate determination of the distributions of the calculated population inversion and temperature in the crystal. The temperature dependence of the emission spectra can then be taken into account as well, which defines the achievable gain of the amplifying media. The resulting calculations' influence on the simulated output beam quality and gain for these active media is presented.

Keywords: Laser Simulation, Solid State Lasers, SCF amplifier, Nd:YAG, Yb:YAG

1. INTRODUCTION

The physical properties of a gain medium strongly influence a laser's output power and beam quality. This manifests in response to the temperature distribution within the gain medium associated with the heat generated during the pumping cycle. However, often overlooked when simulating laser performance are the gain-medium's spectroscopic dependence upon temperature — typically estimated with an effective value — or the spectral characteristics of the pump and/or laser light. While in general such assumptions are reasonable, in cases where there are significant changes in the temperature of the active region, i.e., in cases of highly intense pumping or for cryogenically cooled gain media where the temperature dependence of the spectral properties is stronger, improved accuracy can be achieved with the inclusion of the spectroscopic temperature dependence. Key parameters include the absorption coefficient for the pump light, the stimulated emission cross section, and in cases where the laser transition suffers re-absorption, the absorption cross section for the laser light. These dependencies were measured and reported for Nd:YAG in[1,2,3] and for Yb:YAG in,[4,5] respectively.

In this paper, we show how the temperature dependence of two prominent laser crystals' cross-section and thermo-optic properties can be taken into account when simulating their performance as amplifiers. First, it was necessary to process the measured cross-section data[1,2,3,4,5] to ensure it was clean enough to be suitable for the simulation. Second, a fully 3-dimensional simulation model was set up, which will be explained in Section 2.2, solving multiple coupled systems that include raytracing for the pump propagation, heat flow calculations through Finite Element Analysis (FEA), along with the rate equation analysis for the excited state population density associated with the developing laser field in response to the pump field. The result is that the population inversion can be discretized on a 3-dimensional finite-volume grid, from which the effective local gain can be defined. In the case of amplifiers, the seed can either be described by Gauss modes or by the spectral method of

Send correspondence:
Souryadeep Saha: sourya.saha@fau.de

plane waves. As the seed propagates through the 3-dimensional grid, the gain depends on the local population inversion and temperature dependent stimulated emission cross-section. The output power is finally calculated from the electric field amplitude of the seed at the end of the amplifier.

2. SIMULATION MODEL

2.1 Temperature and wavelength spectroscopic dependencies

The absorption (σ_{abs}) and emission cross sections (σ_{ems}) of two popular gain materials commonly used in laser, or amplifiers, in function of their temperature were measured by Yoon et al.,[1,3] and Körner et al.,[4,5] for Nd:YAG and Yb:YAG, respectively. The spectral range for the measured data covers the entire band associated with the primary energy levels of interest for these materials. In some sections there was a relatively large noise component, e.g., as shown in Figure 1, due to the detection sensitivity limits associated with spectrally weak features. As such, it was necessary to process the data before using it in the simulations. In addition, negative values in the data were set to an infinitesimal positive number, e.g., 10^{-8} pm^2, to ensure they represent physically meaningful values. To fit the data, a linear interpolation, or even a polynomial interpolation, was not feasible due to the sharp spectral peaks; instead, a spline interpolation technique was employed. To get an accurate representation of the stronger peaks and not lose information about the weaker ones, a large number of splines were required. These data files with two dimensions - temperature and wavelength - became too large to be handled efficiently by the software, i.e., each dataset was greater than 3MB in size. To reduce the number of data points, and in effect the size of the files, an adaptive grid method was used. This method selects which data points to keep depending on an acceptable variation between adjacent points. A binary-tree structure was used to traverse the data and compare them, reducing the number of data points from more than 10,000 σ_{abs} data points for each temperature to less than 2000. The processed data is shown in Figure 2. There was no loss of information since these data points represented the peaks accurately while discarding the ranges where the data remained relatively constant. This was only possible after removing the noise from the data. The resulting reduced data files were approximately 300 kB and allowed for reasonable computational efficiency. Subsequently, the absorption cross-section data was converted to a concentration dependent absorption coefficient to be used as the initial starting conditions for raytracing simulation.

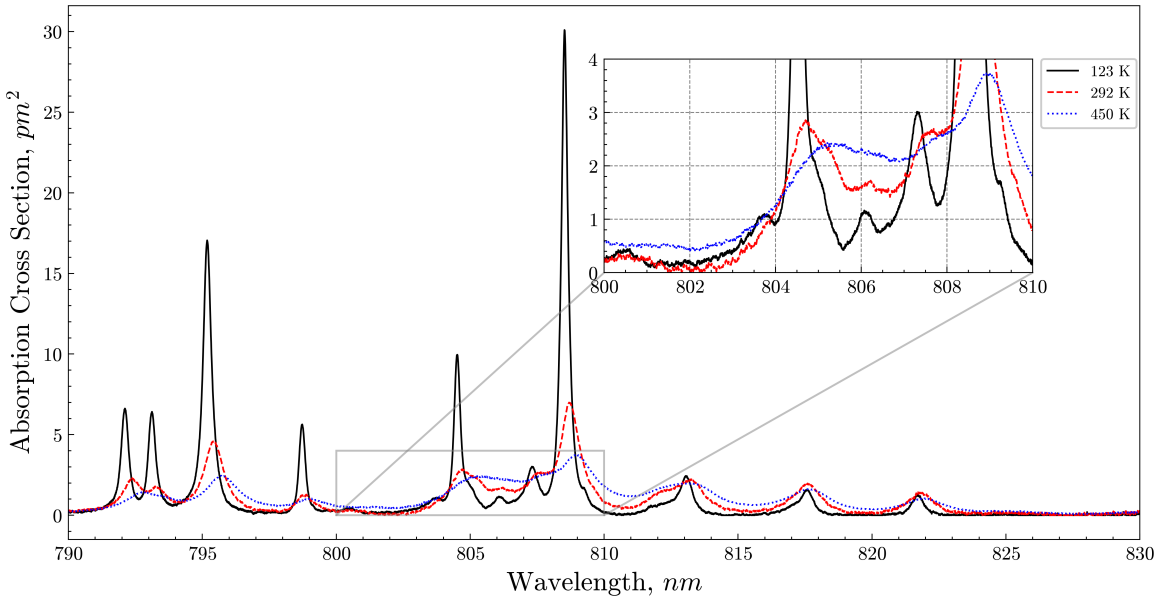

Figure 1: Spectroscopic data for absorption cross-section of Nd:YAG at different temperatures as measured by Yoon et al.[1]

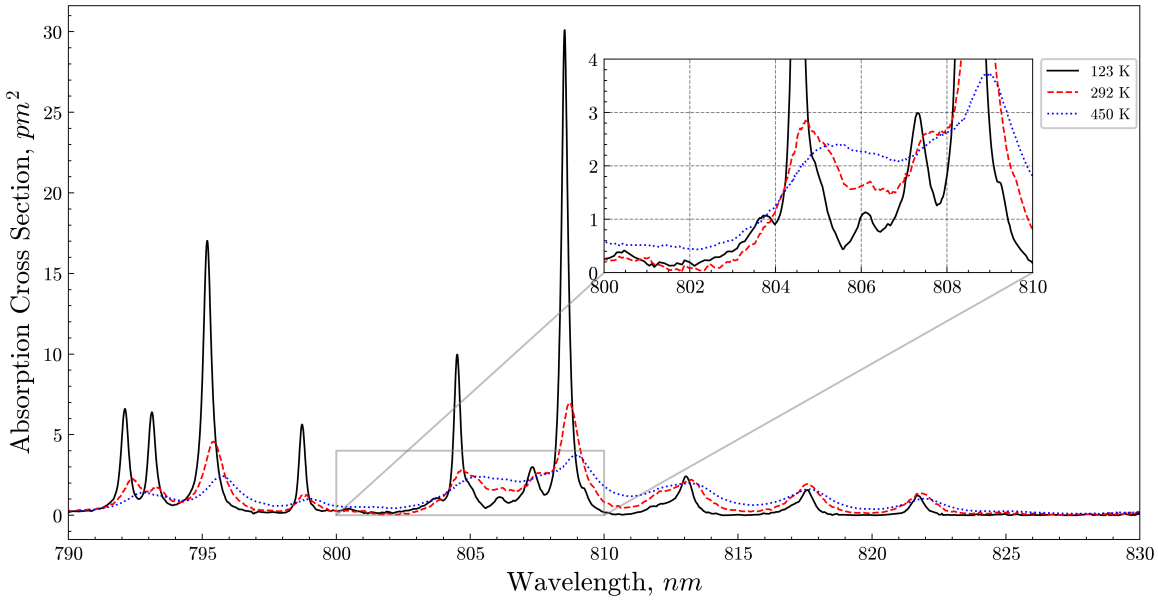

Figure 2: Filtered absorption cross-section data used in calculations for the simulations, following the application of spline fitting and the adaptive grid method to the data shown in Figure 1.

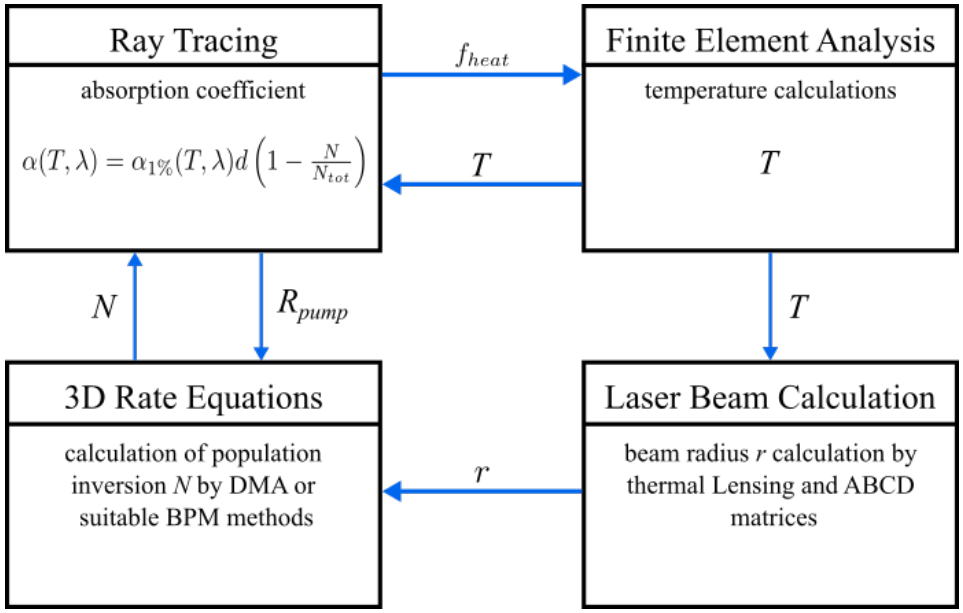

Figure 3: Iterative scheme used to simulate the performance of laser resonators or amplifiers.

2.2 3D Simulation Model

The main spectroscopic parameters of active crystals that depend on wavelength and temperature are:

- absorption cross-section: $\sigma_{abs}(T, \lambda_{pump})$,
- stimulated emission cross-section: $\sigma_{ems}(T, \lambda_{laser})$, and
- in the case of a finite population density in the lower laser level, the re-absorption cross-section for the laser light: $\sigma_{abs}(T, \lambda_{laser})$,

where $T(x, y, z)$ is the temperature inside the laser crystal referenced to the 3-dimensional coordinates (x, y, z), λ_{pump} and λ_{laser} are the wavelengths of the pump and laser light, respectively. The local absorption coefficient $\alpha(x, y, z)$, can then be calculated from σ_{abs}. Analytical functions describing $T(x, y, z)$ depend upon the gain medium geometry, its cooling configuration, and the pump-light distribution within, and as such is often unique to the laser configuration. A generalised solution for the temperature distribution $T(x, y, z)$ can be calculated numerically, for which FEA is an efficient algorithm. To this end, the heat source f_{heat} induced by the pump light has to be calculated by a raytracing algorithm. To achieve this the absorption coefficient at 1 at. % doping is chosen as a reference, $\alpha_{1\%}(T_0, \lambda)$, determined from the absorption cross section for the crystal's initial temperature $\sigma_{abs}(T_0, \lambda_{pump})$, and followed by an iterative calculation, used to calculate both local $T(x, y, z)$ and absorption coefficient $\alpha(T, \lambda)$. This iterative process is depicted in Figure 3.

In the simulation of specific gain media, the actual doping level must be accounted for, i.e., with N_{tot} being the total ion concentration corresponding to the relative doping concentration, d, referenced to a 1 at. % doping. Furthermore, in the case where there is a significant population inversion, ground-state bleaching will also affect the absorption coefficient of the pump light. This effect can be modelled as follows:

$$\alpha(x, y, z) = \alpha_{1\%}(x, y, z)\ d(x, y, z)\ \left(1 - \frac{N(x, y, z)}{N_{\text{tot}}}\right), \tag{1}$$

The dependency of α on N is therefore defined by saturation effects and the local temperature. Moreover, the distribution of the population inversion $N(x, y, z)$ depends upon the pumping rate R_{pump}, which also has to be calculated by raytracing of the pump light. However, in the case of pump light with a finite bandwidth, different formulae are needed for the calculation of the heat source f_{heat} and the pumping rate R_{pump}, which correspond to the results of the raytracing. For example, a broadband spectrum occurs in case of sunlight[6] or flashlamp[7] pumping. The corresponding formulae are:

$$f_{\text{heat}} = \sum_{\lambda_{\text{pump}} \leq \lambda_{\text{laser}}} P_{\text{abs}}(\lambda_{\text{pump}}) * \left(1 - \frac{\lambda_{\text{pump}}}{\lambda_{\text{laser}}}\right) + \sum_{\lambda_{\text{pump}} > \lambda_{\text{laser}}} P_{\text{abs}}(\lambda_{\text{pump}}) \quad \text{and} \tag{2}$$

$$R_{\text{pump}} = \sum_{\lambda \leq \lambda_{\text{laser}}} P_{\text{abs}}(\lambda) / E_{\text{photon}}(\lambda), \tag{3}$$

where $P_{\text{abs}}(\lambda_{\text{pump}})$ is the absorbed pump power at the pump wavelength λ_{pump}. This value can be calculated by raytracing using the absorption coefficient $\alpha(T, \lambda_{\text{pump}})$.

Since the calculation of population inversion $N(x, y, z)$ requires the calculation of the pumping rate R_{pump} by raytracing using the absorption coefficient α defined in Equation (1), an additional iterative algorithm is needed (see Figure 3). The 3-dimensional calculation of population inversion can be performed by different techniques. In case of a laser resonator, Dynamic Mode Analysis (DMA) can be used.[8] Whereas for an amplifier, 3-dimensional Gaussian beam amplification[9] or a BPM method based on the spectral method of plane waves can be applied.[10]

This model is more complex than any model not considering the temperature dependence of σ_{abs} and σ_{ems}, and requires multiple recalculations before reaching a stable state.

3. SIMULATION RESULTS

3.1 Single crystal fiber laser amplifier

SCF amplifiers represent a gain media geometry suited to high-power amplification.[11] Capitalising on pump guiding along the crystals' length, high intensity pumping can be realised. While the SCF dimensions ensures a good cooling efficiency, there is still potential for significant temperature excursions at the centre of the crystal when utilising high pump powers. Consequently, the resulting gain will be strongly linked to saturation effects and the temperature dependence of the spectroscopy for the specific SCF. Here we test the simulation model for Nd:YAG and Yb:YAG SCF amplifiers. The key differences between these gain media is that Yb:YAG is affected by re-absorption at 1030 nm and therefore sensitive to temperature through re-absorption loss. Whilst the four-level transition at 1064 nm for Nd:YAG is not as susceptible to these additional losses, rather the gain

in Nd:YAG will be dominated by the reduced cross sections, for the pump and laser wavelengths, at elevated temperatures.
For initial illustration purposes SCF amplifier setups were configured with the following parameters. The schematics are shown in Figure 4.

- A common length was selected for the SCFs, that is 40 mm, along with a diameter of 1 mm and 1$at.\%$ doping. The SCFs were cooled with a thin film cooling having a heat transfer coefficient of 0.02 W/m^2K.
- Continuous wave (CW) pump with power of 50 W with 0.2 mm width was used.
- The seed beam had 1 W CW power with beam waist within the crystal of 0.3 mm.

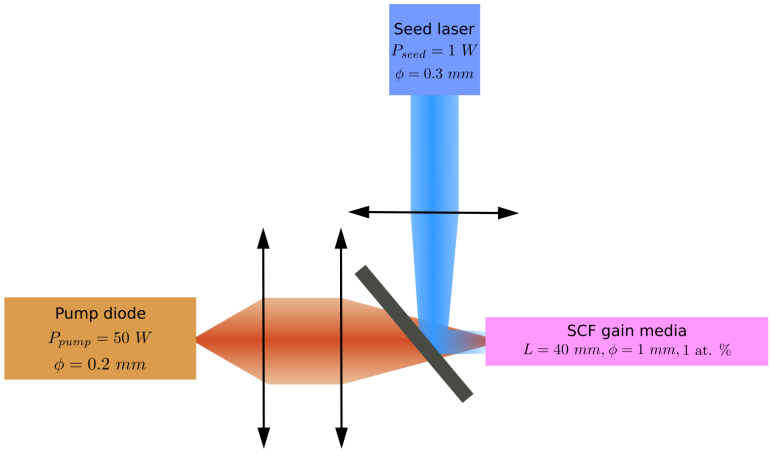

(a) Co-propagating scheme.

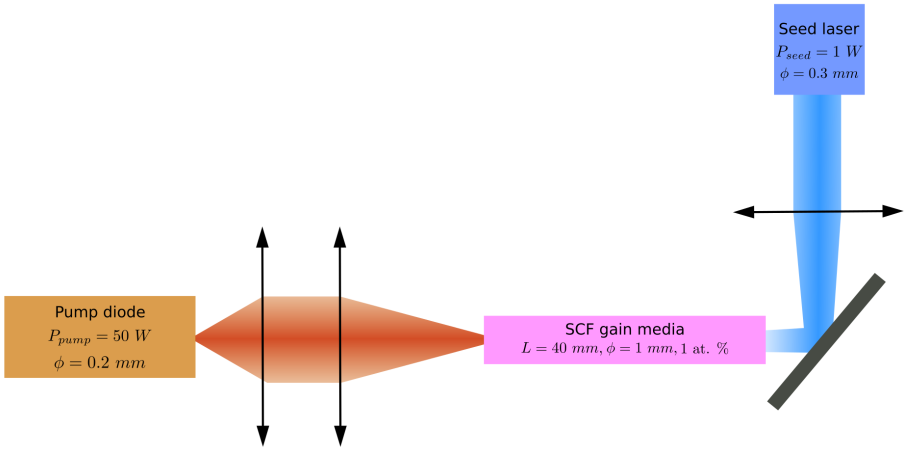

(b) Counter-propagating scheme.
Figure 4: Schematic of the SCF amplifier setup used in the simulations.

Similar SCF amplifiers have been studied before in different research groups.[12,13,14,15] First, we will present some general simulation results and then compare the simulation model with an experimental setup presented by Piehler et al.[15]

The SCF amplifier setup was simulated for different cases, with and without temperature dependent $\sigma_{abs}(\lambda_{pump})$, $\sigma_{ems}(\lambda_{laser})$ and $\sigma_{abs}(\lambda_{laser})$ independently. The ambient temperature was set to 293 K, with saturation effects within the crystal accounted according to Equation (1). The results are presented in Table 1 and Table 2 for

Nd:YAG and Yb:YAG SCFs, respectively. In the two general cases simulated, the pump was setup with a narrow spectral width of 0.5 nm FWHM, to minimise its spectral dependence on σ_{abs}. To illustrate the impact of accounting for the spectroscopic temperature dependence, the calculated output power for the simulated SCF amplifiers were determined by 'switching' on, or off, the specific temperature dependent calculations, as shown in the respective tables.

Nd:YAG SCF

For the neodymium-doped SCF, the model used a pump with a central wavelength of 808.5 nm. The SCF amplifier setup was simulated for both co-propagating and counter-propagating pump and seed configurations.

Table 1: Influence of temperature dependent pump absorption ($\sigma_{abs}(T)$) and stimulated emission cross-section ($\sigma_{ems}(T)$) on output power and beam quality in a 1% doped Nd:YAG SCF for co-propagating and counter-propagating pump and seed configurations.

Pump and seed direction	$\sigma_{abs}(T)$	$\sigma_{ems}(T)$	P_{out} (W)	M^2 $(x \mid y)$		Max. T (K)
Co-propagating	No	No	25.2	18.1	18.1	486.6
	No	Yes	16.8	17.2	17.0	470.5
	Yes	No	26.0	16.0	15.9	465.3
	Yes	Yes	20.5	14.3	14.1	419.0
Counter-propagating	No	No	27.5	5.5	5.5	574.9
	No	Yes	23.8	5.3	5.3	556.8
	Yes	No	28.2	5.7	5.7	490.0
	Yes	Yes	25.3	5.5	5.5	465.4

It was observed that using a counter-propagating system always produced higher gain and better beam quality than co-propagating. It must be noted that the calculation of the M^2 factor was done using BPM.[16] In the case of the co-propagating configuration, the highest value for the calculated gain obtained was, for when including (switching on) the absorption cross section temperature dependence, $\sigma_{abs}(T)$, while maintaining a constant value for σ_{ems}. Whereas it decreased by 35% when including the temperature dependence for the emission but not for the absorption. Instead including both $\sigma_{ems}(T)$ and $\sigma_{abs}(T)$ the gain was 21% lower than the maximum calculated.

In the case of the counter-propagating scheme, a gain of 14.4 dB was obtained with constant values for the absorption and emission cross section. This gain increased by 2.5% when taking into account $\sigma_{abs}(T)$ only. Whereas accounting for both $\sigma_{ems}(T)$ and $\sigma_{abs}(T)$ the gain decreased by 8%. Interestingly, the calculated maximum temperature is lowest in the case of simulating with temperature dependent σ_{abs} and σ_{ems}. This is assumed to be due to a reduced absorbed-power density associated with the diminishing absorption coefficient with increasing temperatures.

Yb:YAG SCF

Since the advantages of the counter-propagating configuration have already been shown, the influence of a finite spectral distribution of the seed, in addition to the spectroscopic temperature dependence, is presented for the Yb:YAG SCF amplifier in Table 2. Two types of input seed lasers were simulated; a single wavelength, and a Gaussian spectrum with a FWHM of 15 nm. Whereas, the pump was modelled with a central wavelength of 940 nm and a bandwidth of 0.5 nm.

It was observed that simulating the amplifiers with the broadband seed resulted in an overall decrease in gain by around 20%. This confirms the importance of accounting for the seed's spectral shape. Furthermore, it was noted that the beam quality of the amplified beam also degraded when considering the broader-bandwidth, lower coherence-length, seed. The effect of the local temperature modelled by switching on the $\sigma_{abs}(T, \lambda_{pump})$, $\sigma_{ems}(T, \lambda_{laser})$ and $\sigma_{abs}(T, \lambda_{laser})$ were between $3-5\%$, due to the relatively small increase in temperature within the crystal, unlike that of the Nd:YAG SCF discussed previously.

Table 2: Influence of temperature dependent pump absorption ($\sigma_{abs}(T, \lambda_{pump})$), stimulated emission cross-section ($\sigma_{ems}(T, \lambda_{laser})$) and re-absorption cross-section ($\sigma_{abs}(T, \lambda_{laser})$) on output power and beam quality in a 1% doped Yb:YAG SCF for counter-propagating pump configuration with single wavelength and Gaussian spectrum seed.

Seed spectra	$\sigma_{abs}(T, \lambda_{pump})$	$\sigma_{ems}(T, \lambda_{laser})$	$\sigma_{abs}(T, \lambda_{laser})$	P_{out} (W)	M^2 $(x \mid y)$		Max. T (K)
Single Wavelength	No	No	No	22.9	1.6	1.6	305.5
	No	No	Yes	23.4	1.6	1.6	309.4
	No	Yes	No	22.2	1.6	1.6	305.4
	No	Yes	Yes	21.7	1.6	1.6	305.3
	Yes	No	No	21.5	1.6	1.6	304.0
	Yes	No	Yes	23.4	1.6	1.6	308.8
	Yes	Yes	No	22.2	1.6	1.6	305.4
	Yes	Yes	Yes	22.7	1.6	1.6	308.7
Gaussian Spectrum (FWHM 15 nm)	No	No	No	18.4	1.9	1.9	305.4
	No	No	Yes	18.8	1.9	1.9	309.4
	No	Yes	No	17.7	1.9	1.9	305.4
	No	Yes	Yes	17.3	1.9	1.9	305.9
	Yes	No	No	15.9	2.0	2.0	302.8
	Yes	No	Yes	18.9	1.9	1.9	308.8
	Yes	Yes	No	17.7	1.9	1.9	305.4
	Yes	Yes	Yes	17.9	1.9	1.9	308.8

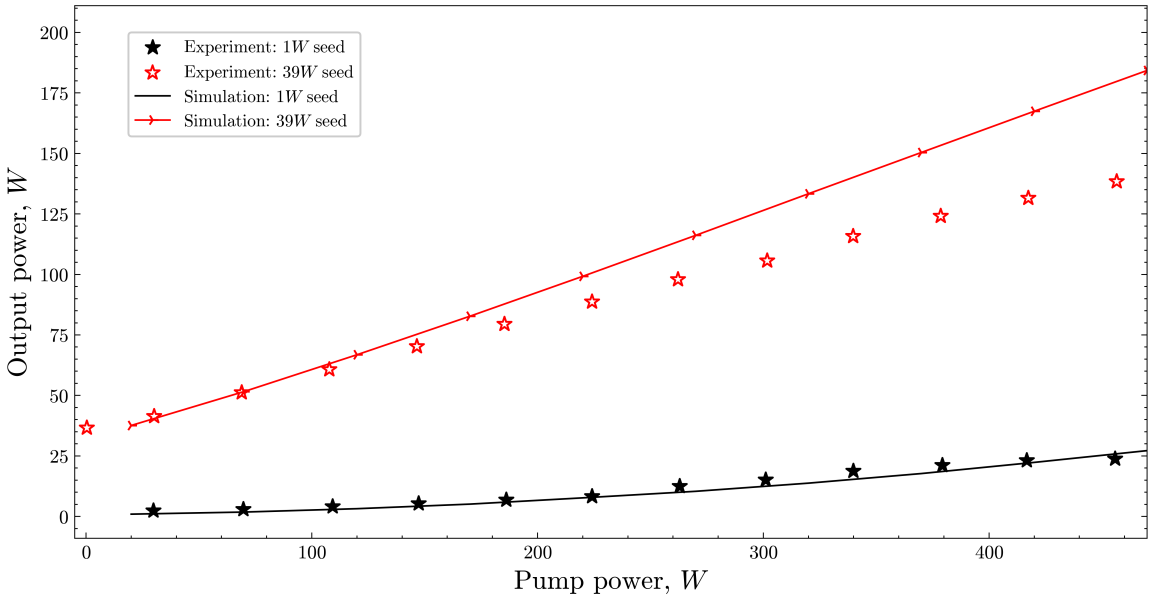

Figure 5: Comparison of the simulation model with experimental data reported in Piehler et. al.[15]

Comparison with reported high-power Yb:YAG SCF amplifier performance

To test the simulation model against reported high-power experimental results we setup the simulated SCF amplifier as described in Piehler et. al.[15] The details of the setup are as follows.

- Yb:YAG SCF with a length of 40 mm, diameter of 1 mm and 1$at\%$ doping. Although the cooling arrangements were not detailed in,[15] the simulation model assumed that the SCF was cooled through a thin interface material having a heat transfer coefficient of 0.02 W/m^2K.
- CW pump with power of 20 - 520 W and 0.6 mm diameter at the entrance facet of the SCF. It is assumed

that the pump's central wavelength was 940 nm with a Gaussian spectrum and 3.5 nm FWHM bandwidth, trying to emulate that of typical pump diodes at this wavelength.

- The CW seed beam power was set to either 1 W or 39 W, with a beam waist within the crystal of 0.4 mm and co-propagating with the pump.

The comparison between the simulation models and the experimental results is presented in Figure 5. It can be seen that for the 1 W seed, the simulation follows closely the reported experimental results. This is implies that through the inclusion of the temperature dependent spectroscopy, the simulation is capturing the effective gain characteristics very well. However, for the 39 W seed the simulation model differs from the experimental results. Piehler et al.[15] demonstrated a maximum amplified output power for their 1 W seed of 23 W, whereas their 39 W seed was amplified to 139 W. In simulation the maximum calculated powers, with and without temperature dependent parameters, are tabulated in Table 3. It shows that the simulation overestimates the power by around 10% for the lower-power seed and some 27% for the higher-power seed. This larger deviation may be attributed to differences in the characteristics of the respective seeds, e.g., beam quality and their respective intensity distributions, spectral content, and in the encountered losses and lensing within the SCF.

Table 3: Influence of temperature dependent pump absorption ($\sigma_{abs}(T, \lambda_{pump})$), stimulated emission cross-section ($\sigma_{ems}(T, \lambda_{laser})$) and reabsorption cross-section ($\sigma_{abs}(T, \lambda_{laser})$) on output power in a $1at.\%$ doped Yb:YAG SCF for a co-propagating pump configuration with single wavelength. Pump power was 450 W.

P_{seed} (W)	$\sigma_{abs}(T, \lambda_{pump})$	$\sigma_{ems}(T, \lambda_{laser})$	$\sigma_{abs}(T, \lambda_{laser})$	P_{out} (W)
1	No	No	No	32.1
	No	No	Yes	32.1
	No	Yes	No	25.8
	Yes	No	Yes	31.2
	Yes	No	No	31.2
	Yes	Yes	Yes	25.2
39	No	No	No	190.3
	No	No	Yes	190.3
	No	Yes	No	179.3
	Yes	No	Yes	187.9
	Yes	No	No	188.0
	Yes	Yes	Yes	177.5

4. CONCLUSION

An iterative scheme involving a raytracing algorithm and FEA that incorporates the temperature dependencies in the spectral properties of two well known gain media is presented in this paper. The model was used to simulate the performance of neodymium and ytterbium-doped YAG SCFs amplifiers and compared with reported configurations from the literature. Compared to using static values for the cross sections, there is a 20% reduction in the calculated gain when $\sigma_{abs}(T)$ and $\sigma_{ems}(T)$ are included for the Nd:YAG SCF amplifier. This is attributed to the high temperatures expected with the intense pumping and large quantum defect between pump and signal for these SCFs. Instead, the spectral dependence of $\sigma_{ems}(T)$ and $\sigma_{abs}(T)$ in Yb:YAG SCF play a more significant role, especially in cases of relatively broad bandwidths that would be consistent with ultra-short-pulse seeds, and must be included in the simulations. The model was also compared to experimental results representing state-of-the-art high-power operation of single-stage SCF amplifiers. Although it could capture the gain behaviour for the lower powered seed of 1 W, there was a 27% discrepancy for a 40-times more powerful seed. It is assumed that this could be due to the differences in the seeds' characteristics. More comparisons with experimental results are planned to show the effectiveness of the model.

ACKNOWLEDGMENTS

SS acknowledges Erlangen Graduate School in Advanced Optical Technologies (SAOT) for their financial support. JM acknowledges the U.K. Engineering and Physical Sciences Research Council (EPSRC) for financial support

via the grant EP/P027644/1. We acknowledge Advanced Software for Laser Design GmbH (ASLD) for the simulation software.

REFERENCES

[1] Yoon, S. J. and Mackenzie, J. I., "Implications of the temperature dependence of Nd:YAG spectroscopic values for low temperature laser operation at 946 nm," SPIE Laser Sources and Applications II **9135**, 913503 (2014).

[2] Yoon, S. J. and Mackenzie, J. I., "Cryogenically cooled 946nm Nd:YAG laser," Optics Express **22**, 8069 (Mar 2014).

[3] Yan, R., Yoon, S. J., Beecher, S. J., and Mackenzie, J. I., "Measuring the elevated temperature dependence of up-conversion in Nd:YAG," IEEE Journal of Selected Topics in Quantum Electronics **21**(1), 329–336 (2015).

[4] Koerner, J., Vorholt, C., Liebetrau, H., Kahle, M., Kloepfel, D., Seifert, R., Hein, J., and Kaluza, M. C., "Measurement of temperature-dependent absorption and emission spectra of Yb:YAG, Yb:LuAG, and Yb:CaF_2 between 20°C and 200°C and predictions on their influence on laser performance," Journal of the Optical Society of America B **29**, 2493 (8 2012).

[5] Körner, J., Jambunathan, V., Hein, J., Seifert, R., Loeser, M., Siebold, M., Schramm, U., Sikocinski, P., Lucianetti, A., Mocek, T., and Kaluza, M. C., "Spectroscopic characterization of yb3+-doped laser materials at cryogenic temperatures," Applied Physics B **116**, 75–81 (9 2013).

[6] Lando, M., Kagan, J., Linyekin, B., and Dobrusin, V., "A solar-pumped nd:yag laser in the high collection efficiency regime," Optics Communications **222**(1), 371–381 (2003).

[7] Koechner, W., [Solid State Laser Engineering], Springer (2006).

[8] Wohlmuth, M., Pflaum, C., Altmann, K., Paster, M., and Hahn, C., "Dynamic multimode analysis of q-switched solid state laser cavities," Optics Express **17**, 17303–17316 (Sep 2009).

[9] Pflaum, C. and Springer, R., "Mode dependent laser pulse amplification: A computational approach in 3d," Conference on Lasers and Electro-Optics , JW2B.5, Optica Publishing Group (2020).

[10] Schmidt, J. D., [Numerical Simulation of Optical Wave Propagation], vol. PM199, SPIE (2010).

[11] Sangla, D., Martial, I., Aubry, N., Didierjean, J., Perrodin, D., Balembois, F., Lebbou, K., Brenier, A., Georges, P., Tillement, O., and Fourmigué, J.-M., "High power laser operation with crystal fibers," Applied Physics B **97**, 263–273 (Oct 2009).

[12] Martial, I., Balembois, F., Didierjean, J., and Georges, P., "Nd:yag single-crystal fiber as high peak power amplifier of pulses below one nanosecond," Optics Express **19**, 11667–11679 (Jun 2011).

[13] Markovic, V., Rohrbacher, A., Hofmann, P., Pallmann, W., Pierrot, S., and Resan, B., "100W class compact Yb:YAG single crystal fiber amplifier for femtosecond lasers without CPA," in [Solid State Lasers XXV: Technology and Devices], Clarkson, W. A. and Shori, R. K., eds., **9726**, 972609, International Society for Optics and Photonics, SPIE (2016).

[14] Lesparre, F., Martial, I., Didierjean, J., Gomes, J. T., Pallmann, W., Resan, B., Loescher, A., Negel, J.-P., Graf, T., Ahmed, M. A., Balembois, F., and Georges, P., "High-power Yb:YAG single-crystal fiber amplifiers for femtosecond lasers," in [Solid State Lasers XXIV: Technology and Devices], Clarkson, W. A. and Shori, R. K., eds., **9342**, 934203, International Society for Optics and Photonics, SPIE (2015).

[15] Piehler, S., Délen, X., Didierjean, J., Aubry, N., Graf, T., Ahmed, M. A., Balembois, F., and Georges, P., "High power amplification in yb:yag single crystal fibers," in [2013 Conference on Lasers_Electro-Optics Europe_International Quantum Electronics Conference CLEO EUROPE/IQEC], 1–1 (2013).

[16] Neubert, B. and Eppich, B., "Influences on the beam propagation ratio m2," Optics Communications **250**(4), 241–251 (2005).